Heterogeneous dynamics on the microsecond scale in simulated $Ni_{0.5}Zr_{0.5}$ metallic melts far below the glass temperature

H. Teichler
Institute for Materials Physics and SFB 605, University of Goettingen, D-37077 Goettingen, Germany
(Received 17 February 2004; revised manuscript received 22 October 2004; published 22 March 2005)

From molecular dynamics simulations for up to 2.5 μs, results are reported on structural dynamics in glass-forming metallic $Ni_{0.5}Zr_{0.5}$ melts at 700 and 785 K. After elimination of high-frequency fluctuations, cascades of atoms and avalanches of atom chains, local in space and time, are identified as complex processes that govern the heterogeneous low-frequency dynamics in sufficiently aged structures near the glass temperature.

DOI: 10.1103/PhysRevE.71.031505 PACS number(s): 64.70.Pf, 61.20.Ja, 61.20.Lc

I. INTRODUCTION

During the liquid-to-glass transition a dramatic slowing down of structural relaxation takes place in the vitrifying melt, yielding a change in the dynamics from liquid to solidlike. Following the idea of Adam and Gibbs [1], the slowing down often is attributed to increasingly cooperative dynamics in the system accompanied by an increasing spatial dynamical heterogeneity (e.g., [2–4]). Dynamical heterogeneity and cooperative behavior have been verified experimentally [2–5] at temperatures around the experimental glass-transition temperature T_G and in molecular dynamics (MD) simulations [6–12] for relaxed melts around T_C, the critical temperature of the mode coupling theory (MCT) [13]. T_C describes a transition from high-temperature dynamics in the melt by homogeneous viscous flow to low-temperature dynamics by thermally activated events in a pseudoarrested state. T_G means the caloric transition temperature visible, for example, by a jump in the specific heat. T_G usually is found below T_C and shows marked cooling-rate dependence [14,15], reflecting the kinetic, nonequilibrium features of the caloric transition.

Early MD computer simulations revealed heterogeneous dynamics in the liquid above and around T_C in form of coherent motions of chains or rings of atoms [16–18], while single-atom translation motion turned out to be increasingly suppressed with decreasing temperature. Experimental substantiation of this picture was obtained, for example, in metallic glasses from diffusion experiments [19], where the extreme low isotope effect gives strong support for the assumption of coherent motions of groups of atoms as fundamental processes. More recent analysis of MD studies regarding spatial distribution of the most mobile (resp. most immobile) atoms in undercooled liquids proved that particles with enhanced mobility aggregate into clusters, within which atom motions take place in a correlated manner along stringlike paths [11]. Closer inspection revealed that during the motion along the paths the degree of coherence depends on the length of the strings in the way that for longer strings the motion is coherent only in shorter segments [11]. The latter "microstrings" seem to correspond to the mobile atom chains observed earlier.

A further type of cooperative dynamics in undercooled liquids has been considered recently by Garrahan and Chandler [20] in their "nontopographic" description of dynamics. They adopt the idea of dynamical facilitation [21], according to which mobile particles in a microscopic region of space influence the dynamics of atoms in neighboring regions, by making them mobile and allowing, in this way, propagation of mobility through the sample. Dynamical facilitation and the MD results of clusters of mobile atoms have been brought together by assuming that the clusters of highly mobile particles are formed as a result of mobility propagation facilitated through quasi-one-dimensional stringlike arrangements [11].

While these approaches are concerned with the dynamical heterogeneity in the undercooled melt, we here shall consider whether and how solidlike behavior results from these pictures under further cooling the system. Solidlike behavior, expected for a well-relaxed amorphous state around and below T_G, implies in essence that structural changes take place as rare processes on a meso- or macroscopic time scale. Dynamical heterogeneity around and below T_G is of particular interest, since Glotzer [9] discussed evidence for a divergence in the spatial extension of mobile clusters in undercooled liquids when approaching the Kauzmann temperature T_K from above, where T_K is discussed in the literature [14,22] as the lower limit of the experimentally accessible caloric glass temperature T_G.

In order to get insight into the corresponding microscopic dynamics in vitrifying metallic systems, we have carried out long-time molecular dynamics simulations on the microsecond scale for a binary $Ni_{0.5}Zr_{0.5}$ model in its glass-forming regime at 700 and 785 K. Extending the simulations from the usual nanosecond to the microsecond scale is like opening a window to study a new dimension. It makes visible the dynamics of processes from which nanosecond-scale simulations depict only short segments such as momentary snapshots. For a simulated, suitably aged vitrifying model of the $Ni_{0.5}Zr_{0.5}$ melt at 700 K, preliminary analysis [23,24] of the early 1.2 μs of the evolution path gives rise to the picture that irreversible (or extreme low-frequency) dynamical cooperativity takes place in terms of avalanches, localized in space-time, and formed by cooperatively acting, correlated transitions of atom chains, mutually triggering and mutually stabilizing each other [23]. By "suitably aged" we mean a system with an α-relaxation time larger than 1 μs. Below we shall present the results of a more detailed analysis of comparable data, which now extend over a significantly longer range of time.

In the following, we shortly describe our simulation model and some of its properties. For characterizing the dynamics of the simulated system on the microsecond scale and allowing comparison with higher-temperature short-time data, we then present the self-part of the intermediate scattering function and the time-averaged mean-squares displacement in the time window from 10^{-14} to some 10^{-6} s at 700 K and above. The further results are concerned with the analysis of the irreversible dynamics and atomistic processes that take place on the microsecond scale.

II. METHOD AND MODEL

The MD simulations are carried out for a binary $Ni_{0.5}Zr_{0.5}$ model. NiZr stands for the broad class of glass-forming binary transition-metal (TM) systems [25] built from small, late, and large early TM atoms. Our results rely on isothermal-isobaric (N,T,p) simulations for a $Ni_{0.5}Zr_{0.5}$ model [26–28] with atomic couplings adapted to *ab initio* hybridized nearly-free-electron–tight-binding-bond calculations [29] and a volume-dependent energy term that models the electron-gas effect of the *s*- and *p*-electron systems. For 648 atoms in a periodically repeated box, the equations of motion are numerically integrated as in our earlier simulations by a fifth-order predictor-corrector algorithm with time step 2.5×10^{-15} s at fixed temperature, the latter being measured by the mean kinetic energy.

The considered temperatures are below the critical temperature T_C of the MCT [13], found at 1120 K for the present $Ni_{0.5}Zr_{0.5}$ model [26,27]. 700 K even is below its Kauzmann temperature found at $T_K=750$ K [28].

III. RESULTS

A. Intermediate scattering function and averaged mean-square displacement

As first result, Fig. 1(a) displays the self-part of the intermediate scattering function (ISF),

$$\mathbf{\Phi}_A(\mathbf{q},\tau) := \langle\!\langle \exp\{i\mathbf{q}\cdot(\mathbf{x}_n(\tau+t)-\mathbf{x}_n(t))\}\rangle\!\rangle_{n\in A}, \qquad (1)$$

for $A=\mathrm{Ni},\mathrm{Zr}$, scattering vector $q=21.6\ \mathrm{nm}^{-1}$ (as used in [26,27]), and temperature $T=700$ K. In addition, the large-time ISF is included for Ni at 785 and 900 K. In Eq. (1), the double brackets mean averages over the particles n of type A and over the evolution time t, with averaging over t up to 3.85 μs at 700 K, 2.45 μs at 785 K, and 1.45 μs at 900 K. As a further quantity we consider in Fig. 1(b) the time-averaged mean-square displacements (averaged MSD)

$$\langle\!\langle r^2(\tau)\rangle\!\rangle_A := \langle\!\langle |\mathbf{x}_n(\tau+t)-\mathbf{x}_n(t)|^2\rangle\!\rangle_{n\in A}. \qquad (2)$$

The double brackets again indicate averaging over the particles of type A and over the evolution time t as described for the ISF.

$\mathbf{\Phi}_A(\mathbf{q},\tau)$ is shown in Fig. 1(a) on a logarithmic τ scale over eight decades. It displays the expected features well

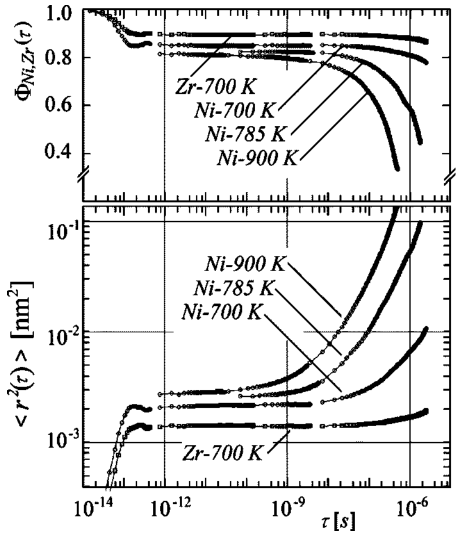

FIG. 1. (a) Self-part of the intermediate scattering function in simulated $Ni_{0.5}Zr_{0.5}$ for Ni and Zr at 700 K, and long-time part for Ni at 785 and 900 K. (b) The time-averaged mean-square displacement in simulated $Ni_{0.5}Zr_{0.5}$ for Ni and Zr at 700 K, and long-time part for Ni at 785 and 900 K.

known for metallic glasses from a number of simulations (e.g., [11,12,19,26,27]), which means an initial decay below some 10^{-13} s due to atom vibrations, an extended plateau regime, and the late β regime indicating the onset of the final α decay. For 700 and 785 K, the α-decay time τ_α is outside the range of data displayed in the figure. By fitting a stretched exponential law to the ISF curves, τ_α can be estimated as $\tau_\alpha(700\ \mathrm{K})\approx10^{-4}$ s, $\tau_\alpha(785\ \mathrm{K})\approx2\times10^{-6}$ s, and $\tau_\alpha(900\ \mathrm{K})\approx7\times10^{-7}$ s.

The $\mathbf{\Phi}_A(\mathbf{q},\tau)$ curves should be compared with earlier results for the same $Ni_{0.5}Zr_{0.5}$ model [26,27]. In [26,27], the concentration-averaged intermediate-scattering functions $\mathbf{\Phi}(\mathbf{q},\tau)=0.5\times(\mathbf{\Phi}_{\mathrm{Ni}}(\mathbf{q},\tau)+\mathbf{\Phi}_{\mathrm{Zr}}(\mathbf{q},\tau))$ were presented for a series of temperatures on a time window up to τ around 1 ns. At τ near 1 ns, they indicate for $\mathbf{\Phi}(\mathbf{q},\tau)$ a plateau value of 0.862 at 700 K and of 0.832 at 800 K [26]. These data are in reliable accordance with values following from the present data, 0.870 for $\mathbf{\Phi}(\mathbf{q},\tau)$ at 700 K and 0.847 at 785 K.

The long, flat plateau at 700 and 785 K, extending from 10^{-11} to 10^{-8} s (respectively 5×10^{-9} s), indicates that there are, in essence, no persistent changes in the atomic arrangement for delay times in this interval. The flatness of the plateau implies, for the short-time fluctuations, visible by the decay below and around 10^{-12} s, that they are reversible excitations only, or else they would add up to a slow decay in the β regime, as found in the present 900-K curve for Ni. A final slope in the β regime of the intermediate scattering function is well known for temperatures around and above T_C. It is demonstrated in a number of simulations for rather different systems, such as models of undercooled metallic melts, e.g., NiZr [26,27] or CuZr [31], molten SiO_2 [32], or the Lennard-Jones [30] and the Dzugutov liquid [11]. In all these cases, the finite slope in the β regime demonstrates a marked, continuous adding up of irreversible structural changes from the atomistic time scale to the α decay. On the

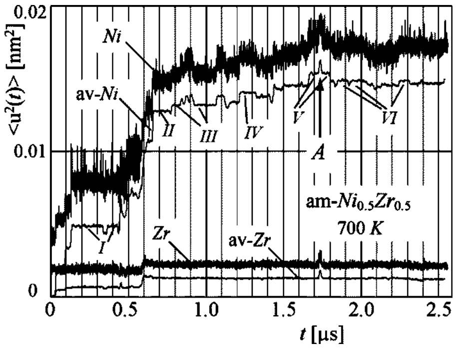

FIG. 2. Mean-square displacements in simulated amorphous $Ni_{0.5}Zr_{0.5}$ at 700 K from original atomic dynamics (Ni, Zr) and from low-frequency filtered dynamics (av-Ni, av-Zr). The plateaus I–VI indicate classes of equivalent configurations.

other hand, existence of a flat plateau has been already demonstrated for the $Ni_{0.5}Zr_{0.5}$ model [26] at 700 and 800 K.

The basic features depicted in Fig. 1(b) for $\ll r^2(\tau)\gg_A$, the time-averaged MSD, are in accordance with the behavior known for this quantity at temperatures around and above T_C (e.g., [11,33,34]). Clearly visible is the ballistic and vibrational τ^2 regime, an overshooting before entering the early β regime, the subdiffusive transient region in the range of the late β regime, and the final approach towards a diffusive, linear-τ dependence. A special feature is the flat part of the β regime in the 700- and 785-K curves, which reflects the properties already discussed in context with the flat part in the corresponding ISF. In the $\ll r^2(\tau)\gg_A$, the onset of deviation from flat behavior in the late part of the β regime is rather clearly visible, yielding an onset time of 4×10^{-9} s at 700 K and 5×10^{-8} s at 785 K.

B. Microscopic processes at 700 K

Both quantities considered in Sec. III A reflect time averages over particular microscopic processes. In the present section we are looking for the atomistic, microscopic details of the underlying events. In order to make visible effects of the individual events, we use, as in [23,24], the mean-squares displacement without averaging along the evolution path, that is,

$$u^2(t,t_0)_A := \langle|\mathbf{x}_n(t+t_0) - \mathbf{x}_n(t_0)|^2\rangle_{n\in A}, \tag{3}$$

where the simple brackets denote averages over the particles of type A and t_0 means an initial reference time with configuration $\{\mathbf{x}_n(t_0)\}$. Figure 2 presents the related MSD for $T=700$ K along the evolution path up to 2.5 μs with $\{\mathbf{x}_n(t_0)\}$ generated from a well-relaxed 980-K configuration of our previous studies [26,27] by further cooling it with a rate of 10^{10} K/s.

The spiky structure of the MSD curves in Fig. 2 is due to reversible short-time fluctuations in the atomic positions, such as thermal vibrations of the atoms or overbarrier motions of isolated atoms or groups of atoms between competing equilibrium configurations in the rather rigid matrix of surrounding material [23,24]. The intermittent dynamics visible by the spikes was recently related to the cage effect, which reflects the approach towards the arrested state of the MCT [35]. It is known from the work of Shlesinger, Klafter, and Zumofen [36] that a fractal dimension of waiting times, hidden behind the intermittent dynamics in undercooled melts, gives rise to the power-law decays, e.g., in the time-averaged MSD. Such features are not accessible in the present analysis, as they would require much longer simulation time beyond the microsecond range. However, for diffusion in glassy solids below T_G and well below T_C, it is known from experiments [19] that particle penetration follows the laws of Brownian motion.

In order to extract the long-time fluctuations and irreversible structural changes hidden behind these motions, we introduce time-averaged atomic positions as special diagnostic tool,

$$\mathbf{y}_n(t) := \int dt'\, g(t-t')\mathbf{x}_n(t'), \tag{4}$$

$$g(t) = \exp[-1/2(t/\tau_0)^2]/\sqrt{2\pi\tau_0^2}. \tag{5}$$

For our purpose $\tau_0=3$ ns turns out to be appropriate, yielding that in the $\mathbf{y}_n(t)$ all motions are averaged out that reversibly take place on a time scale short against 3 ns, while the evolution of the configurations $\{\mathbf{y}_n(t)\}$ presents the long-time, low-frequency dynamics of the amorphous structure, in particular the processes relevant for vitrification of the melt.

Figure 2 also includes the MSD corresponding to the $\mathbf{y}_n(t)$,

$$\overline{u^2}(t,t_0)_A := \langle|\mathbf{y}_n(t+t_0) - \mathbf{y}_n(t_0)|^2\rangle_{n\in A}. \tag{6}$$

As to be expected, the $\overline{u^2}(t,t_0)_A$ remain close to zero at short times, as the thermal vibrations are suppressed in these curves, and they follow the gross features of the $u^2(t,t_0)_A$ at larger times.

The $\overline{u^2}(t,t_0)_A$ curves display plateaus of constant $\overline{u^2}(t,t_0)_A$ values reflecting nearly constant configurations $\{\mathbf{y}_n(t)\}$. In Fig. 2, some of the plateaus are denoted by I, II, III, etc. Our further analysis refers to changes between the related configurations and uses these changes to characterize the low-frequency evolution of the structure.

Changes between configurations at t_1 and t_2 are analyzed by comparing, for example, the averaged atomic positions at the selected times with help of the displacements

$$\Delta\mathbf{y}_n(t_2,t_1) := \mathbf{y}_n(t_2) - \mathbf{y}_n(t_1). \tag{7}$$

A typical example for the distribution of displacement values Δy is shown in Fig. 3, presenting in a semilogarithmic plot the probability function $P(\Delta y)$ of displacements versus $\sqrt{\Delta y}$ deduced from our simulations for the case $t_1=0.7$ μs, $t_2=1.73$ μs. [$P(\Delta y)$ is evaluated by creating a histogram of the atomic displacements with a channel width of 0.0195 nm and dividing the number of atoms in each channel by half the distance between the two nearest channels with nonvanishing number of atoms.] The atomic displacements during the selected time interval of 1 μs extend up to 0.41 nm. $P(\Delta y)$ decreases strongly at intermediate values 0.01 nm $<\Delta y$ <0.09 nm, where the linear slope in the plot indicates non-Gaussian decay. At larger values $\Delta y>0.09$ nm an excess

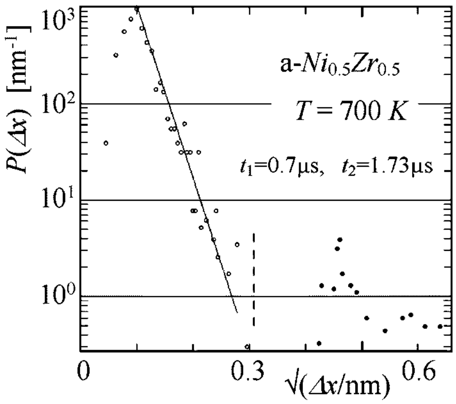

FIG. 3. Probability distribution of displacement values Δy between the times t_1 and t_2 vs $\sqrt{\Delta y}$.

contribution is found in $P(\Delta y)$ due to a few distinguished atoms with displacements above this value. In the following these atoms shall be named shortly "transferred" atoms.

In order to characterize the distribution in space, Fig. 4(a) displays by straight lines the atomic displacements $\Delta \mathbf{y}(t_2, t_1)$ in the selected time interval projected onto the drawing plane. In Fig. 4(a) are included the (projected) positions $\mathbf{y}_n(t_2)$ of the transferred atoms, symbolized by light gray circles for Ni atoms, dark gray for Zr.

The transferred atoms form groups in space, as demonstrated by Fig. 4(a). From analyzing a series of (t_1, t_2) pairs, the pattern of the transferred atoms turns out as a rather robust signature of the structural change. The plateaus of nearly constant $\overline{u^2}(t)_A$ values, labeled as I–VI in Fig. 2, indicate classes of equivalent configurations in the way that for two configurations from the same class, there are no transferred atoms at all, while when comparing configurations

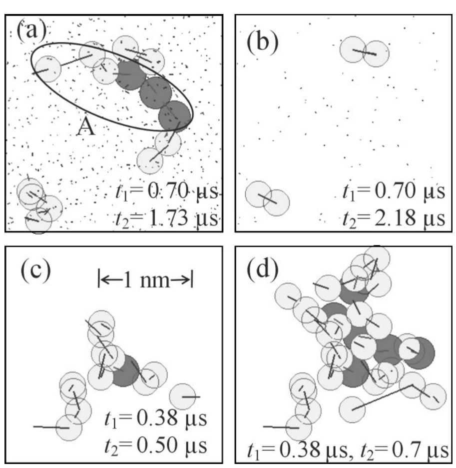

FIG. 4. Atomic displacements between times t_1 and t_2 from low-frequency filtered dynamics. The lines indicate the displacements. The circles mean the positions at t_2 of transferred atoms with displacements larger than 0.09 nm (light gray, Ni; dark gray, Zr atoms). (a) Reversible chain displacement [for atom group A (see text)]. (b) Pairs of two-particle exchanges. (c) The initial part of an avalanche breakthrough. (d) The avalanche of irreversibly displaced atoms. [In (c) and (d) the displacements of only the transferred atoms are shown for clarity.]

from two different classes, the topology of the pattern of transferred atoms remains the same, independent of the selected class members.

Figure 4(b) shows the projected pattern for $t_1 = 0.7$, $t_2 = 2.18$ μs. It is characterized by mere particle exchanges within two pairs of adjacent Ni atoms. According to this, between 1.73 and 2.2 μs a marked relaxation takes place, which eliminates most of the displacements seen in Fig. 4(a). The individual processes in the formation and decay of the pattern can be related to individual steps in the smoothed MSD in Fig. 2. For example, the left-hand flank of peak A in Fig. 2 corresponds to displacement of group A of atoms encircled in Fig. 4(a), while the right-hand flank reflects the return of these atoms.

A behavior different from Figs. 4(a) and 4(b) is seen in Figs. 4(c) and 4(d). Figure 4(c) corresponds to $t_1 = 0.38$, $t_2 = 0.5$ μs. It indicates a chain of displaced Ni and Zr atoms, similar to Fig. 4(a). Unlike the latter, the pattern in Fig. 4(c) does not relax, but is followed by an avalanche of further structural changes as illustrated by Fig. 4(d), depicting transferred atoms between $t_1 = 0.38$, $t_2 = 0.7$ μs. The avalanche drives the system from one metastable configuration to a second one. As can be inferred from Figs. 4(a) and 4(b), the second one is rather stable over about 1.5 μs of further evolution of the system, up to temporary excitations and particle exchange processes.

The present findings support the picture that at 700 K in the considered system, irreversible—or low-frequency—structural changes take place by exchange processes or by avalanches and cascades of transferred atoms, where the latter mean reactions between else reversible fluctuations in the system. Processes of this type seem to form the mechanism to relate the structural dynamics in the solidlike state below the experimental T_G to the fluctuation dynamics around T_C. Interpretation of irreversible dynamics as a result of interactions between reversible fluctuations already has been proposed by Argon and Shi [37] in the discussion of viscoplastic deformations under load, where they attribute it to elastic interactions between ellipsoidal deformation centers.

C. Low-frequency processes at 785 K

When we consider avalanches as particular vehicles of irreversible local structure changes at 700 K, the question is raised on how the system, with increasing temperature, turns into a common undercooled melt. In order to approach this, we display in Fig. 5(a) MSD curves from "averaged" atomic positions $\{\mathbf{y}_n(t)\}$ at 785 K. Avalanches are reflected by steps in the curves as demonstrated by Figs. 5(b) and 5(c). Figure 5(b) shows an avalanche that starts at 0.74 μs with the rare event of a chain displacement in the Zr subsystem, as can be deduced from Fig. 5(a), followed by a cascade in the Ni subsystem. Figure 5(c) provides one with mainly Ni atoms. A comparison of Figs. 5(b) and 5(c) clearly shows that different regions of the melt are concerned by these avalanches. Closer inspection of the data shows that, for example, also the steps at 0.8 and 0.98 μs are the traces of avalanches of clusters of 27 and 36 transferred atoms. The steps in the time range between these avalanches, however, reflect a series of

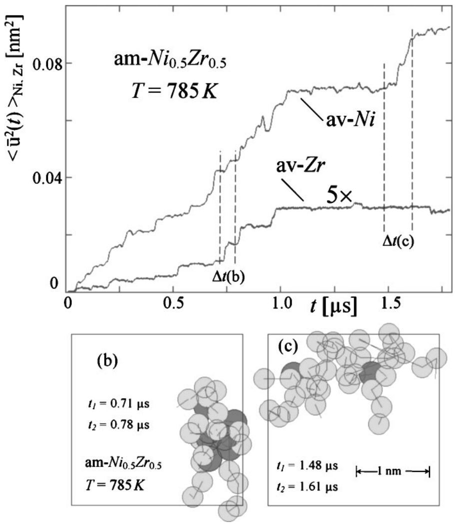

FIG. 5. (a) Mean-squares displacements from low-pass filtered atomic dynamics at 785 K (Zr curve enlarged five times). Δt(b) and Δt(c): time intervals for the displacements in panels (b) and (c). (b) The pattern of transferred atoms in the avalanche between 0.71 and 0.78 μs, starting with a chain of displaced Zr atoms followed by a Ni cascade. (c) The transferred atoms in the avalanche between 1.48 and 1.61 μs.

successive chainlike processes (with six, nine, and nine transferred atoms in the steps). The chains apparently stabilize each other and prepare the conditions for the final, catastrophic event at 0.98 μs.

As obvious from Fig. 5(a), at 785 K, the frequency of avalanches and cascades is much higher than at 700 K. They, moreover, group together in time, forming active periods and periods of calmness. This grouping together becomes more pronounced at higher temperatures, as can be inferred, for example, from the MSD data [23] at 900 K. The data indicate superavalanches consisting of series of successive avalanches separated by periods of calmness.

IV. DISCUSSION AND CONCLUDING REMARKS

The present paper is concerned with irreversible, low-frequency dynamics in a simulated undercooled, well-relaxed, and suitably aged vitrifying $Ni_{0.5}Zr_{0.5}$ MD model system. Suitably aged here means a system with α relaxation time larger than 1 μs. Our analysis of the ISF and the time-averaged MSD shows that under this condition there is a separation of about three orders of magnitude in time between high- and low-frequency dynamics for the present model. The negligible slope of the ISF and of the MSD in the region between high- and low-frequency processes indicates a negligible probability for structural fluctuations with decay times in this time window. The negligible slope also indicates that the high-frequency dynamics reflect reversible processes only. This situation is markedly different from the dynamics at higher temperatures in the commonly considered undercooled liquids, e.g., around T_C, where high- and low-frequency processes are much less separated in time and continuously merge together, yielding a marked probability of decay processes for all decay times.

By elimination of the high-frequency dynamics through low-pass filtering, we made visible the traces of low-frequency processes, which in essence provide the irreversible structural changes in the solidifying melt on mesoscopic times. For the 700 K structure, three processes of different type have been found: particle exchange events, a chainlike motion, and an avalanche process. While the isolated chainlike motion turned out as a reversible, thermally activated excitation only, the exchange events and the avalanche process indicate long-living structural changes, resembling irreversible processes on the present microsecond scale. The particle exchange events in their effects are comparable to the ring process [38–40]. But while the latter were introduced as coherent excitations in the system [40], the exchange events here seem to be the irreversible remainders of a sequence of complex processes.

The formation of the avalanches as an irreversible result of interacting processes of atom-chain motions, mutually triggering and stabilizing each other, has been discussed in our earlier study [23]. The present treatment now is able to follow the formation process in some detail. Our analysis indicates for the avalanche observed at 700 K and, e.g., for the avalanches at 785 K in Figs. 5(a) and 5(b), that they start with a stringlike atom-chain motion, followed by a series of further atomic displacements in the form of moving chains of atoms or cascades of atoms, until apparently a new metastable configuration is reached.

It is tempting to identify the avalanches with the regions of dynamic facilitation recently used by Garrahan and Chandler [20] in their nontopographic description of dynamics in supercooled liquids. We must state, however, that avalanches in the present system, e.g., the one at 700 or the one at 785 K around 1.6 μs, mean local events in space *and* time, forming from metastable configurations and ending up in long-living metastable configurations of the system.

The low-frequency analysis of the 785-K data reveals further details. There, on the one hand, avalanche processes are found. On the other hand, a series of stringlike chain transitions takes place, where the chains follow each other with a delay of about 25 ns. Although this process ends up in a final avalanche, it may be considered as an indication how dynamics by stringlike chain transitions and by avalanches merge together and how by such processes mobility is transported through the system. The 785-K data provide the link between our findings at 700 K and the picture of heterogeneous dynamics in undercooled liquids at temperatures around T_C, sketched, e.g., in the recent study on particle dynamics and the development of stringlike motion in the supercooled Dzugutov liquid [11] or the investigation of spatially heterogeneous dynamics and dynamic facilitation in simulated viscous silica [12].

Although there is a close interrelationship between the 785-K data and the various pictures for the dynamics in the supercooled melts at higher temperature, there is a significant difference towards the behavior at 700 K, below the Kauzmann temperature T_K. The 700-K data substantiate the idea that at this temperature the structural dynamics take place by individual, irreversible events separated in space and time, where the avalanche turned out as a promising example of such a process. (The second type of processes, the particle exchange, is of minor importance for structural dynamics. It may be of importance, however, regarding the diffusion of particles.) It is the price paid for the necessary ultralong simulations of the rather immobile system that the 700-K data do not allow statistical sampling over the processes. However, at least for the present sample there are clear indications that heterogeneous dynamics below T_{K} are characterized by events separated in space and time.

Clearly, the detailed structure of intermittent dynamics visible in the present MSD of smoothed atomic positions will average out for larger samples. However, for larger samples, there are observations [41] that volume elements of present size as fractions of the larger system show fluctuations similar to those described here. This corroborates the idea that in larger systems, the dynamics can be considered as a superposition of avalanches and cascades, localized in space and time like the present ones, which locally induce intermittent dynamics but which show smooth behavior when averaging over mesoscopic volume elements. At this point our treatment comes into contact with the energy landscape interpretation [42–44] of the complex mechanical properties and thermodynamics of glasses. Our results support the assumption that there exist long-living metastable configurations of the structure, forming mesobasins in the energy landscape, around which the commonly studied transitions among different energy basins take place as rapid, mainly reversible fluctuations. Our treatment visualizes in space the changes between adjacent mesobasins in terms of the related transferred atoms pattern.

For the well-relaxed TM system around its Kauzmann temperature, our results support the view that the irreversible avalanches and cascades promote the proceeding vitrification and isothermal relaxation of the structure. The proceeding vitrification may be characterized by a decreasing probability for such events. In this context, vibrations and coherent overbarrier motions of individual atom chains turned out as reversible excitations only, in agreement with the increasing reversibility at decreasing temperature observed for atom-chain motions by simulations in the melt [45]. Concerning the low-frequency behavior of glass-forming, undercooled metallic melts, it is tempting to relate the additional wing of loss processes found recently on the high-frequency side of the α peak in the mechanical loss spectrum of a ternary, metallic Zr glass near T_{G} [46] to complex, low-frequency processes like the present avalanches.

The present results demonstrate explicitly how, in a metallic-bonded system, macroscopic relaxation times emerge, even in presence of the unavoidable large density of high-frequency thermal fluctuations. Regarding processes with decreasing temperatures, our observations provide a smooth link between the phenomenon of flow in the undercooled melt and isolated dynamical events, local in space and time, characteristic for a finite-temperature solid. We shall not rule out that in less-relaxed samples irreversible structural dynamics and relaxation take place by overbarrier motions of individual chains of atoms until the chain system has reached a metastable equilibrium. Rejuvenation [47,48] of the glassy state by shear deformations may be one way to generate such less-relaxed samples.

[1] G. Adam and J. H. Gibbs, J. Chem. Phys. **43**, 139 (1965).
[2] E. J. Donth ,*The Glass Transition* (Springer, Berlin 2001).
[3] M. Ediger, Annu. Rev. Phys. Chem. **51**, 99 (2000).
[4] H. Sillescu, J. Non-Cryst. Solids **243**, 81 (1999).
[5] E. R. Weeks and D. A. Weitz, Phys. Rev. Lett. **89**, 095704 (2002).
[6] D. Caprion, J. Matsui, and H. R. Schober, Phys. Rev. Lett. **85**, 4293 (2000).
[7] C. Donati, J. F. Douglas, W. Kob, S. J. Plimpton, P. H. Poole, and S. C. Glotzer, Phys. Rev. Lett. **80**, 2338 (1998).
[8] R. Yamamoto and A. Onuki, Phys. Rev. Lett. **81**, 4915 (1998).
[9] S. C. Glotzer, J. Non-Cryst. Solids **274**, 342 (2000).
[10] N. Giovambattista, S. V. Buldyrev, F. W. Starr, and H. E. Stanley, Phys. Rev. Lett. **90**, 085506 (2003).
[11] Y. Gebremichael, M. Vogel, and S. C. Glotzer, J. Chem. Phys. **120**, 4415 (2004).
[12] M. Vogel and S. C. Glotzer, Phys. Rev. Lett. **92**, 255901 (2004).
[13] W. Götze and L. Sjögren, Rep. Prog. Phys. **55**, 241 (1992).
[14] R. Lück, Q. Jiang, and B. Predel, J. Non-Cryst. Solids, **117/118** 911 (1990).
[15] R. Brüning and K. Samwer, Phys. Rev. B **46**, 11318 (1992).
[16] H. Miyagawa, Y. Hiwatari, B. Bernu, and J. P. Hansen, J. Chem. Phys. **88**, 3879 (1988).
[17] S. Sanyal and A. K. Sood, Europhys. Lett. **34**, 361 (1996).
[18] B. B. Laird and H. R. Schober, Phys. Rev. Lett. **66**, 636 (1991).
[19] F. Faupel, W. Frank, M.-P. Macht, H. Mehrer, V. Naundorf, K. Rätzke, H. R. Schober, S. K. Sharma, and H. Teichler, Rev. Mod. Phys. **75**, 237 (2003).
[20] J. P. Garrahan and D. Chandler, Phys. Rev. Lett. **89**, 035704 (2002).
[21] G. H. Fredrickson and H. C. Andersen, Phys. Rev. Lett. **53**, 1244 (1984).
[22] H. J. Fecht, Mater. Trans., JIM **36**, 777 (1995).
[23] H. Teichler, J. Non-Cryst. Solids **312**, 533 (2002).
[24] H. Teichler, J. Non-Cryst. Solids **293**, 339 (2001).
[25] L. A. Greer, Science **267**, 1947 (1995).
[26] H. Teichler, Phys. Rev. Lett. **76**, 62 (1996).
[27] H. Teichler, Phys. Rev. E **53**, R4287 (1996).
[28] H. Teichler, Phys. Rev. B **59**, 8473 (1999).
[29] Ch. Hausleitner and J. Hafner, Phys. Rev. B **45**, 128 (1992).
[30] W. Kob and H. C. Andersen, Phys. Rev. E **52**, 4134 (1995).
[31] M. Kluge and H. R. Schober, Defect Diffus. Forum **194-199**, 849 (2001).
[32] J. Horbach and W. Kob, Phys. Rev. E **64**, 041503 (2001).
[33] J. Horbach and W. Kob, Phys. Rev. B **60**, 3169 (1999).
[34] W. Kob and H. C. Andersen, Phys. Rev. E **51**, 4626 (1995).
[35] S. C. Glotzer, Y. Gebremichael, N. Lacevic, T. B. Schroder,

and F. W. Starr, Comput. Phys. Commun. **146**, 24 (2002).
[36] M. F. Shlesinger, J. Klafter, and G. Zumofen, Am. J. Phys. **67**, 1253 (1999).
[37] A. S. Argon and L. T. Shi, Acta Metall. **31**, 499 (1983).
[38] Y. Loirat, G. Brebec, Y. Limoge, N. Mousseau, and J. L. Bocquet, Defect Diffus. Forum **194**, 855 (2001).
[39] G. Wahnström, Phys. Rev. A **44**, 3752 (1991).
[40] H. Teichler, Defect Diffus. Forum **143-147**, 717 (1997).
[41] I. Ladadwa and H. Teichler (unpublished).
[42] C. A. Angell, Science **267**, 1924 (1995).
[43] P. G. Debenedetti and F. H. Stillinger, Nature (London) **410**, 259 (2001).
[44] B. Doliwa and A. Heuer, J. Non-Cryst. Solids **307-310**, 32 (2002).
[45] C. Gaukel, M. Kluge, and H. R. Schober, Philos. Mag. A **79**, 1907 (1999).
[46] P. Rosner, K. Samwer, and P. Lunkenheimer, Europhys. Lett. **68**, 226 (2004).
[47] M. Utz, P. G. Debenedetti, and F. H. Stillinger, Phys. Rev. Lett. **84**, 1471 (2000).
[48] K. Brinkmann and H. Teichler, Phys. Rev. B **66**, 184205 (2002).